Applied Surface Science 278 (2013) 101–105

Contents lists available at SciVerse ScienceDirect

Applied Surface Science

journal homepage: www.elsevier.com/locate/apsusc

Ultrafast pulsed laser deposition of carbon nanostructures: Structural and optical characterization

M. Pervolaraki[a,*], Ph. Komninou[b], J. Kioseoglou[b], A. Othonos[c], J. Giapintzakis[a,*]

[a] Nanotechnology Research Center and Department of Mechanical and Manufacturing Engineering, University of Cyprus, 75 Kallipoleos Avenue, P.O. Box 20537, 1678 Nicosia, Cyprus
[b] Department of Physics, Aristotle University of Thessaloniki, GR-54124 Thessaloniki, Greece
[c] Department of Physics, Research Centre of Ultrafast Science, University of Cyprus, P.O. Box 20537, 1678 Nicosia, Cyprus

ARTICLE INFO

Article history:
Available online 14 March 2013

Keywords:
Ultrafast pulsed laser deposition
Carbon nanostructures
Onion-like carbon
Turbostratic carbon

ABSTRACT

Carbon nanostructured materials were obtained by high-repetition rate pulsed laser ablation of a graphite target using a train of 10-ps duration pulses at 1064 nm in different pressures of high-purity Ar gas. It is demonstrated that their microstructure and optical properties vary as a function of the argon pressure. High-resolution transmission electron microscopy revealed the existence of onion-like carbon nanostructures embedded in a matrix of amorphous carbon nanofoam for samples prepared at 300 Pa. In comparison samples prepared at 30 Pa show evidence of both onion-like and turbostratic carbon coexisting in a matrix of amorphous carbon nanofoam whereas samples prepared in vacuum are continuous films of amorphous carbon. Transient transmission spectroscopy measurements suggested that free carrier absorption is the dominant effect following photo-excitation for probing wavelengths in the range of 550–1000 nm and its magnitude varies among the materials investigated due to their different microstructures.

1. Introduction

Devices can potentially become more compact and faster using nanostructures of a single material because scattering caused by defects and interfaces are limited. Carbon nanostructures [1–8] exhibit remarkable electronic, optical and mechanical properties thus they have triggered an increased interest in incorporating them in electronics and optoelectronics applications [9]. For example, it has been shown that onion-like carbon nanostructures can be exploited for the fabrication of supercapacitors to be used in applications that require large bursts of power, long lifetimes and a decent storage capacity [10].

A number of synthesis techniques have been employed for obtaining a variety of nanostructures. For example, heat treatment of carbon shoots [11] or ultra-dispersed nanodiamond [12], CVD method [13], ns pulsed laser deposition of Ni- and Ni-Co-doped graphitic targets [14], laser irradiation of SiC thin films [15] and carbon blacks [16], and more recently laser resonant excitation of precursor ethylene molecules at 10.532 μm [17] have been used for the production of carbon onions. Among these techniques, pulsed laser deposition has been a promising one for the gas phase synthesis of high-purity carbon nanostructures. While there has been a significant amount of published work on using ns [18,19] and fs [20,21] lasers for the production of carbon films and nanostructures, there is a limited number of reports for the case of ps lasers especially in association with high-repetition rate pulses. The ps-domain lies between the thermally dominated ns-regime and the essentially non-thermal fs-regime [5]. Toward this end, we produced carbon nanostructured materials using 10-ps ultrafast pulsed laser deposition (UFPLD) in the presence of high-purity Ar gas. Here we report on their structural and optical properties investigated by high-resolution transmission electron microscopy (HRTEM) and transient transmission spectroscopy, respectively.

2. Experimental

Non-equilibrium plasma of carbon species was produced by 1064 nm irradiation of pristine graphite target from a Nd:YVO_4 laser source at pulse repetition rate of 200 kHz. A train of either 120×10^6 or 360×10^6 pulses with pulse duration (FWHM) of 10 ps and laser irradiance of $\sim 10^{11}$ W cm^{-2} were employed for all experiments. The laser beam angle of incidence was set at 45° with respect to the surface of the continuously rotating and rastering target, in contrast to the experimental configuration (90°) used by Rode et al. [5]; thus, we consider the interaction of the laser beam with the expanding plume negligible (*vide infra*). The target-to-substrate

* Corresponding authors. Tel.: +357 22894502; fax: +357 22895381.
E-mail addresses: pervolaraki@ucy.ac.cy (M. Pervolaraki), giapintz@ucy.ac.cy (J. Giapintzakis).

0169-4332/$ – see front matter © 2013 Published by Elsevier B.V.
http://dx.doi.org/10.1016/j.apsusc.2013.03.015

Table 1
UFPLD deposition conditions for all carbon nanostructures deposited on n-type Si (1 0 0) and quartz substrates.

Sample code	No. of laser pulses	P_{Ar} (Pa)
C93	360×10^6	300
C121	120×10^6	300
C95	360×10^6	30
C127	120×10^6	30
C97	360×10^6	10^{-3}
C125	120×10^6	10^{-3}

separation distance was kept at 4 cm. The PLD chamber was evacuated to a pressure of 10^{-3} Pa prior to introducing the high-purity argon gas. The argon pressure (P_{Ar}) during irradiation of the target was maintained at 30 and 300 Pa. The carbon materials were collected on *n*-type Si (1 0 0) and quartz substrates that were kept at room temperature. The Si substrates were cleaned ultrasonically in acetone, methanol and isopropanol while the quartz substrates were cleaned in acetone and blown with high-purity N_2 gas prior to deposition. The number of deposition pulses and ambient Ar pressure used for the deposition of the samples discussed in this work are shown in Table 1.

The microstructure of a series of carbon samples was investigated by HRTEM. The study was carried out using a JEOL 2011 electron microscope operated at 200 kV with a point resolution of 0.194 nm and C_s = 0.5 mm.

Transient transmission spectroscopy was employed to investigate the carrier relaxation mechanisms of the produced carbon materials on a fs time scale. Measurements were carried out using a typical pump-probe optical setup in a non-collinear configuration where differential transmission was utilized. The ultrafast amplifier system consisted of a self-mode-locked Ti:Sapphire oscillator generating 100 fs pulses at 800 nm and repetition rate of 1 kHz. The amplified pulses were used to generate 400 nm pump pulses using non-linear BBO crystals. A small part of the fundamental energy was also used to generate a super-continuum white light by focusing the beam on a sapphire plate (probe beam).

3. Results and discussion

HRTEM images (Fig. 1a) revealed that sample C93, deposited at P_{Ar} = 300 Pa, consists of an amorphous carbon (*a*-C) nanofoam matrix in which a high density of onion-like carbon (OLC) [10,22] nanostructures are embedded. In Fig. 1b a larger area of a lower magnification image is given where the *a*-C nanofoam matrix is clearly visible. At the center of the image a single OLC nanostructure is presented. The OLCs have an average radius of ~10 nm and an amorphous core. Most of them exhibit a circular or elliptical morphology (in projection). The number of concentric graphitic shells ranges between 4 and 20 and the distance between the shells is 0.335 nm corresponding to the d-spacing of the (0 0 0 2) planes of graphite. In addition to well-dispersed OLCs there are also clusters of multiple OLCs.

Sample C95 (deposited at P_{Ar} = 30 Pa) displays a similar morphology to that of sample C93 as revealed by the HRTEM images of Fig. 1c. It also consists of a matrix of *a*-C nanofoam with embedded OLC nanostructures. The measured spacing of the concentric shells equals to 0.33–0.34 nm close to the spacing of (0 0 0 2) planes of graphite. The density of OLCs is, however, higher compared to C93, and from the areas that we have examined, it is concluded that the proportion between the OLC nanostructures and the matrix in sample C95 is twice the proportion in sample C93. Specifically, in sample C95 18% of the examined area is filled by OLC nanostructures. However, because in many cases clusters of multiple OLCs are observed, an uncertainty of about 5% should be considered on the aforementioned value. Another distinct difference between the two samples is the presence of turbostratic carbon among the OLC structures in sample C95 while the *a*-C nanofoam occupies significantly smaller area. The d-spacing of turbostratic carbon was measured to be 0.4 nm. In Fig. 1d a low magnification HRTEM image of sample C95 is presented. It is evident that the vast majority of the area is filled by turbostratic carbon, while at the right side of the image multiple OLC nanostructures are clearly defined. In addition, those OLC nanostructures exhibit a rather small amorphous core while most of them reveal an elliptical shape. The difference between samples C93 and C95 can be extracted by comparing Fig. 1b and d. The dominant structure in the former case is the a-C nanofoam matrix while in the latter one the turbostratic carbon structure.

The OLC nanostructures reported in this article are an order of a magnitude smaller than those produced using Ni- or Ni-Co-doped graphite target and ns pulses at 248 nm [14]. We believe that in our case we obtain smaller OLC nanostructures due to the low energy of pulses (μJ) used resulting in atomic-like evaporation of the species rather than ejection of precursor droplets by high-energy pulses (100 s of mJ) as in the case of the ns regime (conventional PLD).

The cross-section HRTEM image presented in Fig. 1e revealed that under vacuum conditions a continuous *a*-C film (sample C97) without the presence of any nanostructures was produced. The 17 nm-thick film is clearly seen (the top surface of the *a*-C film is marked by a dashed line in Fig. 1c) due to the difference in the contrast between the film and the amorphous glue on top.

It can be concluded therefore that by varying only one of the deposition parameters, P_{Ar}, it is possible to controllably modify the microstructure of the produced carbon materials. Core–shell OLC nanostructures embedded in an *a*-C nanofoam matrix are produced when high P_{Ar} of 300 Pa is utilized during the deposition process. Higher density of core–shell OLC nanostructures coexist with turbostratic carbon in an *a*-C nanofoam matrix upon the decrease of P_{Ar} to 30 Pa. Compact *a*-C films are created when vacuum conditions are used. The microstructure of the carbon nanostructured materials is independent of the substrate used, an outcome to be expected because the deposition took place at room temperature and the nanostructures were formed in the gas phase (*vide infra*) [23].

Differential transmission measurements of sample C121 (P_{Ar} = 300 Pa) following ultrafast pulse excitation at 400 nm (3.1 eV) and using probing wavelength in the range 500–1000 nm are displayed in Fig. 2a. It is clearly evident from the time-resolved data that there is a fast response after the excitation by the ultrafast pulse, which is pulse-width limited, followed by a much slower recovery toward equilibrium over hundreds of picoseconds. The differential transmission is negative for probing wavelengths longer than 550 nm. This suggests that free carrier absorption is the dominant effect following photo-excitation. The photo-generated carriers undergo secondary excitations to higher energy states induced by the probing laser pulse. This is to be expected given the large number of surface states available in a carbon nanostructured sample. It is pointed out that state filling is observed only for probing wavelength at 500 nm.

Differential transmission measurements of sample C125 (vacuum made) are displayed in Fig. 2b. The results appear to be qualitatively similar with the measurements obtained for sample C121. Even though the two samples were fabricated under different pressures, it is evident than in both cases free carrier absorption is the dominant effect. We can conclude that secondary photo-excitation occurs due to the presence of *a*-C either as a nanofoam matrix that contains OLC nanostructures or as a pure *a*-C continuous film. In addition similar behavior has also been observed in sample C127 (P_{Ar} = 30 Pa). However, the signal was much weaker due to stronger absorption at the probing wavelengths. The stronger absorption of sample C127 (P_{Ar} = 30 Pa) in comparison to that of C121 (P_{Ar} = 300 Pa) could be attributed to

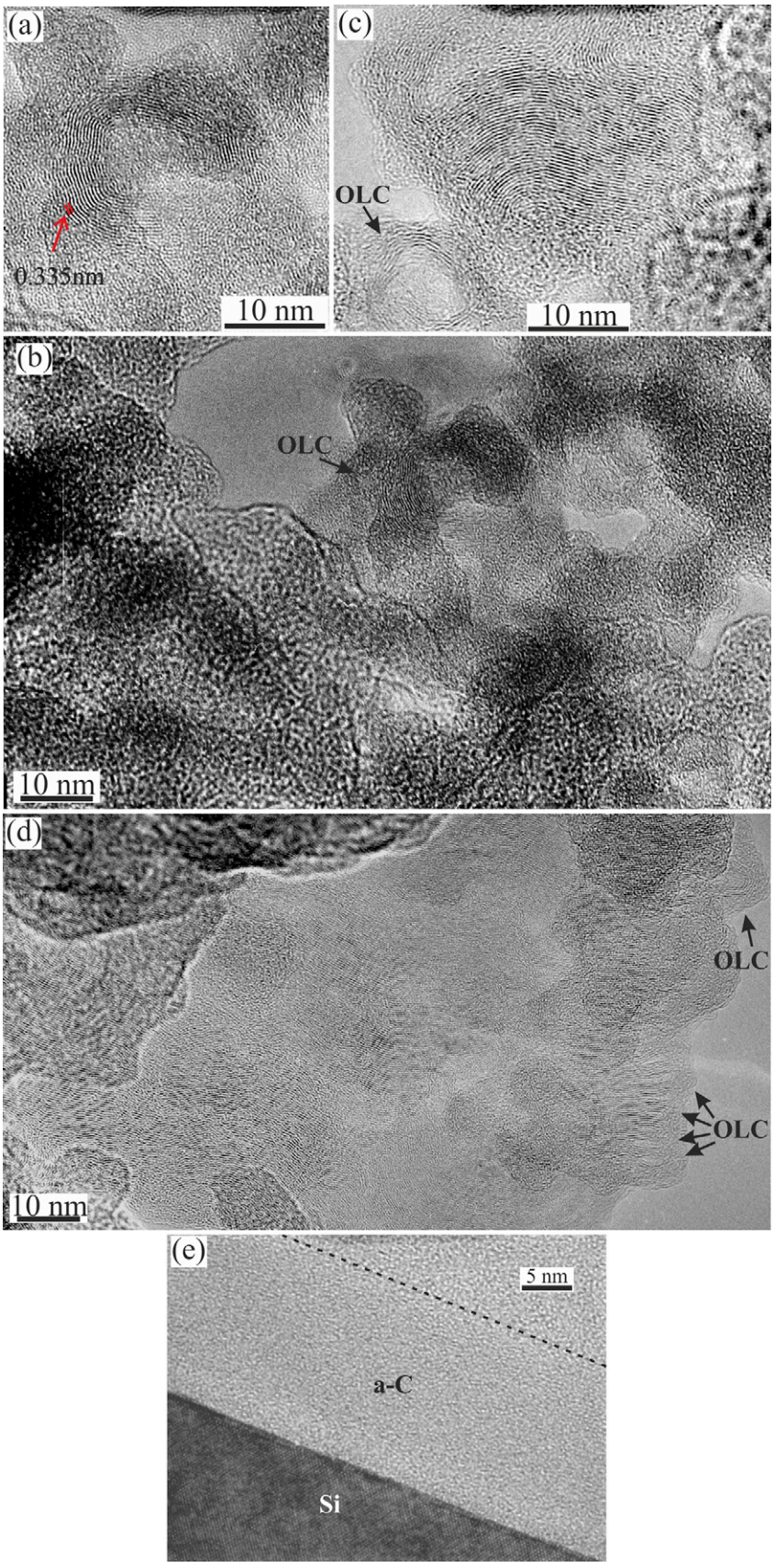

Fig. 1. HRTEM images of carbon nanostructures deposited on Si (1 0 0) substrates. Sample C93 (P_{Ar} = 300 Pa): (a) OLC nanostructure with amorphous core. (b) A HRTEM image, showing the dominant a-C structure as well as the existence of the OLC nanostructures. Sample C95 (P_{Ar} = 30 Pa): (c) concentric OLC nanostructures embedded in *a*-C nanofoam. Turbostratic carbon is depicted at the right part of the image. (d) A larger area showing the turbostratic structure. In addition multiple OLC nanostructures are observed. Sample C97 (vacuum conditions): (e) cross-section HRTEM image illustrating the *a*-C film grown on Si (1 0 0) substrate.

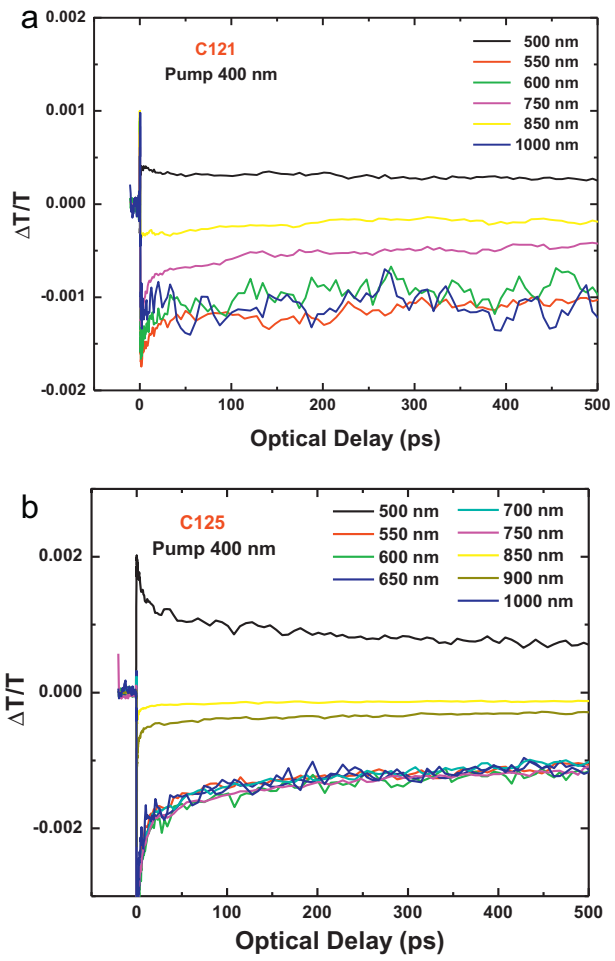

Fig. 2. Transient transmission decays of (a) sample C121 deposited using P_{Ar} = 3 mbar and (b) sample C125 deposited under vacuum conditions, at several probing wavelengths following excitation with 100 fs pulses at 400 nm (3.1 eV).

higher density of OLC nanostructures (twice the proportion) and the highly absorbent turbostratic carbon structure present in the sample. Both, C121 and C127, reveal higher absorption than the vacuum made *a*-C film, C125.

The continuous *a*-C film produced under vacuum conditions is speculated to be formed upon arrival of the high kinetic energy carbon species on the substrate surface. On the other hand, the formation of the highly absorbent OLC nanostructures is believed to occur within the evaporation/ablation plume, where the collision mean free path between C—C and C—Ar atoms is small hence increasing the collision probability [22,24]. The formation of the OLCs depends on a combination of optimum background gas pressure for the formation of carbon clusters and an optimal annealing temperature (~4000 K) for the transformation of the clusters to well-ordered OLCs [23]. According to Lau et al. low argon pressure results in poor aggregation of carbon atoms (small clusters of carbon atoms) and thus incomplete OLC structures due to the long collision mean free path of the evaporated species [23]. The argon pressures used in this work are at the lower end of the desired pressure range for the formation of OLCs, thus explaining the formation of turbostratic carbon from incomplete carbon onions in the case of P_{Ar} = 30 Pa. High repetition rate is believed to have a direct effect on the average target temperature and its evaporation [25]. At the repetition rate of 200 kHz the time interval between pulses is 5 μs and is expected to result in a continuous evaporation of the graphite target and a constant annealing temperature within the plume; conditions that are necessary for the formation of OLC's [23].

Finally, we comment on the laser beam-plume interaction. Rode et al. [2] have experimentally studied the angular distribution of an expanding laser plume during high-repetition rate laser-matter interactions in vacuum, when a spot size of few microns is used. They found that an angular distribution of ~120° is obtained for a spot size of ~50 μm and a target-to-substrate distance of a few centimeters. Therefore, when the laser angle of incidence is ≤30° with respect to the target surface no interaction is expected to take place between the laser pulse and the expanding plume. In our experiments the spot size and the target-to-substrate distance are similar to the values used in Ref. [2], however, the laser beam impinges on the graphite target at 45° with an intensity of 10^{11} W cm^{-2}. Thus under vacuum deposition conditions we expect the laser beam to interact with only a small portion of the evaporated plume. On the other hand, when the evaporation takes place in an Ar atmosphere a narrower angular distribution of the expanding plume is expected. Hence, in this case no interaction of the laser beam with the plume should occur. Furthermore, even in the case of laser beam-plume interaction we consider the expanding plume to be transparent because the incident laser beam intensity used in our experiments is lower than the threshold intensity for vapor ionization and inverse Bremsstrahlung processes to occur [25].

4. Conclusions

Carbon nanostructured materials have been fabricated using single-step bottom-up ps ultrafast pulsed laser deposition with 1064 nm radiation at 200 kHz. HRTEM revealed that the microstructure of the carbon materials depends strongly on the P_{Ar} used during deposition. OLC nanostructures embedded in *a*-C nanofoam matrix and OLCs coexisting with turbostratic carbon in *a*-C nanofoam matrix were obtained using P_{Ar} of 300 and 30 Pa, respectively; whereas, compact *a*-C films were produced under vacuum conditions. Finally, it was found that the absorption in the visible and NIR spectrum increases with increasing density of OLC nanostructures in the *a*-C nanofoam matrix.

Acknowledgements

Financial support from the Strategic Infrastructure Project NEW INFRASTRUCTURE/STPATH/0308/04 of DESMI 2008, which is co-financed by the European Regional Development Fund, the European Social Fund, the Cohesion Fund, and the Research Promotion Foundation of the Republic of Cyprus, is greatly acknowledged.

References

[1] H.W. Kroto, J.R. Health, S.C. O'Brien, R.F. Curl, R.E. Smalley, C_{60}: buckminsterfullerene, Nature 318 (1985) 162–163.
[2] A.V. Rode, E.G. Gamaly, B. Luther-Davies, Formation of cluster-assembled carbon nano-foam by high-repetition-rate laser ablation, Applied Physics A 70 (2000) 135–144.
[3] A.V. Rode, S.T. Hyde, E.G. Gamaly, R.G. Elliman, D.R. McKenzie, S. Bulcock, Structural analysis of a carbon foam formed by high pulse-rate laser ablation, Applied Physics A 69 (1999) S755–S758.
[4] A.V. Rode, R.G. Elliman, E.G. Gamaly, A.I. Veinger, A.G. Christy, S.T. Hyde, B. Luther-Davies, Electronic and magnetic properties of carbon nanofoam produced by high-repetition rate, Applied Surface Science 197/198 (2002) 644–649.
[5] A.V. Rode, B. Luther-Davies, E.G. Gamaly, Ultrafast ablation with high-pulse-rate lasers. Part II. Experiments on laser deposition of amorphous carbon films, Journal of Applied Physics 85 (8) (1999) 4222–4230.
[6] K.S. Novoselov, A.K. Geim, S.V. Morozov, D. Jiang, Y. Zhang, S.V. Dubonos, I.V. Grigorieva, A.A. Firsov, Electric field effect in atomically thin carbon films, Science 306 (2004) 666–669.
[7] A.K. Geim, K.S. Novoselov, The rise of graphene, Nature Materials 6 (2007) 183–191.
[8] X.L. Sheng, Q.B. Yan, F. Ye, Q.R. Zheng, G. Su, T-carbon: a novel carbon allotrope, Physical Review Letters 106 (2011) 4, 155703.

[9] N. Savage, Super carbon graphene is phenomenally strong, thin, flexible, transparent and conductive—and applications beckon, Nature 483 (2012) S30–S31.
[10] D. Pech, M. Brunet, H. Durou, P. Huang, V. Mochalin, Y. Gogotsi, P.L. Taberna, P. Simon, Ultrahigh-power micrometer-sized supercapacitors based on onion-like carbon, Nature Nanotechnology 5 (2010) 651–654.
[11] W.A. de Heer, D. Ugarte, Carbon onions produced by heat treatment of carbon soot and their relation to the 217.5 nm interstellar absorption feature, Chemical Physics Letters 207 (1993) 480–486.
[12] V.L. Kuznetsov, A.L. Chuvilin, Y.V. Butenko, I.Y. Mal'kov, V.M. Titov, Onion-like carbon from ultra-disperse diamond, Chemical Physics Letters 222 (1994) 343–348.
[13] C.N. He, C.S. Shi, X.W. Du, J.J. Li, N.Q. Zhao, TEM investigation on the initial stage growth of carbon onions synthesized by CVD, Journal of Alloys and Compounds 452 (2008) 258–262.
[14] G. Radhakrishnan, P.M. Adams, F.D. Ross, Plume diagnostics and room-temperature deposition of carbon nanotubes and nano-onions at 248 nm, Journal of Physics: Conference Series 59 (2007) 424–427.
[15] T. Gorelik, S. Urban, F. Falk, U. Kaiser, U. Glatzel, Carbon onions produced by laser irradiation of amorphous silicon carbide, Chemical Physics Letters 373 (2003) 642–645.
[16] S. Hu, P. Bai, F. Tian, S. Cao, J. Sun, Hydrophilic carbon onions synthesized by millisecond pulsed laser irradiation, Carbon 47 (2009) 876–883.
[17] Y.S. Zhou, W. Xiong, J. Park, M. Qian, M. Mahjouri-Samani, Y. Gao, L. Jiang, Y. Lu, Laser-assisted nanofabrication of carbon nanostructures, Journal of Laser Applications 24 (2012) 19, 042007.
[18] G. Radhakrishnan, P.M. Adams, L.S. Bernstein, Plasma characterization and room temperature growth of carbon nanotubes and nano-onions by excimer laser ablation, Applied Surface Science 253 (2007) 7651–7655.
[19] W. An, X. Zhao, Z. Zang, R. Su, Carbon dendrite formation induced by pulsed laser irradiation, Applied Surface Science 256 (2010) 2304–2307.
[20] F. Garrelie, N. Benchikh, C. Donnet, R.Y. Fillit, J.N. Rouzaud, J.N. Laval, A. Pailleret, One-step deposition of diamond-like carbon films containing self-assembled metallic nanoparticles, by femtosecond pulsed laser ablation, Applied Physics A 90 (2008) 211–217.
[21] A. Santagata, A. De Bonis, A. De Giacomo, M. Dell'Aglio, A. Laurita, G.S. Senesi, R. Gaudiuso, S. Orlando, R. Teghil, G.P. Parisi, Carbon-Based nanostructures obtained in water by ultrashort laser pulses, Journal of Physical Chemistry C 115 (2011) 5160–5164.
[22] E.G. Gamaly, A.V. Rode, B. Luther-Davies, Formation of diamond-like carbon and carbon foam by ultrafast laser ablation, Laser and Particle Beams 18 (2000) 245–254.
[23] D.W.M. Lau, D.G. McCulloch, N.A. Marks, N.R. Madsen, A.V. Rode, High-temperature formation of concentric fullerene-like structures within foam-like carbon: experiment and molecular dynamics simulation, Physical Review B 75 (2007) 4, 233408.
[24] E.G. Gamaly, N.R. Madsen, D. Golberg, A.V. Rode, Expansion-limited aggregation of nanoclusters in a single-pulse laser-produced plume, Physical Review B 80 (2009) 11, 184113.
[25] E.G. Gamaly, A.V. Rode, B. Luther-Davies, Ultrafast ablation with high-pulse-rate lasers. Part I. Theoretical considerations, Journal of Applied Physics 85 (1999) 4213–4221.